A NOVEL ENHANCED QUANTUM IMAGE REPRESENTATION BASED ON BIT-PLANES FOR LOG-POLAR COORDINATES

XIAO CHEN

School of Computer Science and Engineering, Southeast University, Nanjing, 211189, China.
863210211@qq.com

ZHIHAO LIU

School of Computer Science and Engineering, Southeast University, Nanjing, 211189, China.
Key Laboratory of Computer Network and Information Integration (Southeast University)
Ministry of Education, Nanjing, 211189, China.
lzh@seu.edu.cn

HANWU CHEN

School of Computer Science and Engineering, Southeast University, Nanjing, 211189, China.
Key Laboratory of Computer Network and Information Integration (Southeast University)
Ministry of Education, Nanjing, 211189, China.
hw_chen@seu.edu.cn

LIANG WANG

School of Electronics and Information Engineering, Wuzhou University, Wuzhou, Guangxi, 543003, China.
839083518@qq.com

Quantum image representation has a significant impact in quantum image processing. In this paper, a bit-plane representation for log-polar quantum images (BRLQI) is proposed, which utilizes $(n+4)$ or $(n+6)$ qubits to store and process a grayscale or RGB color image of 2^n pixels. Compared to a quantum log-polar image (QUALPI), the storage capacity of BRLQI improves 16 times. Moreover, several quantum operations based on BRLQI are proposed, including color information complement operation, bit-planes reversing operation, bit-planes translation operation and conditional exchange operations between bit-planes. Combining the above operations, we designed an image scrambling circuit suitable for the BRLQI model. Furthermore, comparison results of the scrambling circuits indicate that those operations based on BRLQI have a lower quantum cost than QUALPI. In addition, simulation experiments illustrate that the proposed scrambling algorithm is effective and efficient.

Keywords: Quantum image representation, Bit-planes, Log-polar coordinate, Image scrambling

1 Introduction

Quantum image processing (QIP), as an emerging research area in quantum information technology and image processing, has attracted widespread attention from scholars [1]-[2]. This mainly relies on the physical properties of quantum coherence, superposition and entanglement, and the ability of qubits to store exponential amounts of data simultaneously [3]. In

general, quantum image processing has the advantages of high computational efficiency and large storage capacity compared with classical image processing.

Quantum image representation (QIR) is a top priority for QIP tasks, as it enables classical information to be stored in a quantum state. Several QIR models (QIRM) have been proposed for representing images using qubits, including Quantum Lattice [4], the flexible representation of quantum images (FRQI) [5], the multi-channel RGB images representation of quantum images (MCQI) [6], and a normal arbitrary superposition state of quantum image (NASS) [7]. These QIRMS use amplitude to encode the pixel information of the image, which improves the coding efficiency and also increases the difficulty of image retrieval. In order to address this issue, a novel enhanced quantum representation (NEQR) is put forward [13], which use a sequence of qubits to encode the image. By improving the coordinate or color coding of the image, a series of new image representation models are generated, such as an improved NEQR(INEQR) [9], a generalized model of NEQR (GNEQR), and a novel quantum representation of color digital images (NCQI) [10]. To further increase the storage capacity, the quantum image representation based on bit-planes (BRQI) [11] and a new quantum representation model of color digital images (QRCI) [12] have been proposed, these two models use a combination of bit plane and color information to encode images. Compared with GNEQR, NEQR and NCQI, the capacity of BRQI and QRCI is increased by 16 times and 2^{18} times, respectively. In addition to image encoding based on amplitude and qubit sequence, some new technologies are applied to image encoding, including a quantum log-polar image (QUALPI) for processing log-polar sampled images [8], and a Fourier transform qubit representation (FTQR) [14] for encoding color information into a quantum superposition state. Furthermore, a novel QIRM [15] is proposed for image brightness and saturation processing.

Quantum image processing algorithms (QIPA) based on different quantum image representation models emerge continually, such as quantum image segmentation [16], quantum image matching [17], quantum image watermarking (QImW) [18], quantum image steganography(QImS) [19]-[20], and quantum image encryption(QImE) [21]-[22]. In addition, image scrambling is also a method often used in image encryption. Among the above studies, QImW, QImS and QImE belong to the research area of quantum information security, which has contributed to the protection of sensitive information.

In order to increase the storage capacity of images sampled in logarithmic polar coordinates, we encode color information in the quantum basis state. Combined with the bit-plane coding method, a novel quantum image representation model BRLQI is proposed, which requires only $(2n + 4)$ qubits to represent a grayscale image with 2^n pixels and $(2n + 6)$ qubits to represent a color image of the same size. The capacity of BRLQI improves 16 times than QUALPI. Furthermore, we propose a number of QIP operations and design a corresponding circuit for image scrambling based on the BRLQI model, including color information complement operation, bit-planes reversing operation, bit-planes translation operation and conditional exchange operations between bit-planes. Analyzing the quantum cost of the above quantum operations, we conclude that those QIP operations based on BRLQI have lower quantum cost than QUALPI.

This paper is organized as follows. Section 2 briefly introduces the preliminary knowledge. Section 3 describes the proposed quantum image representation model QUALPI as well as the procedures of quantum image preparation and retrieving, a series of QIP operations based on

QUALPI are designed for image scrambling in Section 4. Finally, Some notable conclusions are provided in Section 5.

2   Preliminaries

2.1   Quantum gates

Single qubit states $|0\rangle$ and $|1\rangle$ and their dual states $\langle 0|$ and $\langle 1|$ are defined as follows:

$$|0\rangle = \begin{bmatrix} 1 \\ 0 \end{bmatrix}, |1\rangle = \begin{bmatrix} 0 \\ 1 \end{bmatrix}, \langle 0| = \begin{bmatrix} 1 & 0 \end{bmatrix}, \langle 1| = \begin{bmatrix} 0 & 1 \end{bmatrix}. \tag{1}$$

Unitary matrices identity(I), Hadamard(H), NOT gate(X), and $R_x(\theta)$ gates can be expressed as

$$
\begin{aligned}
I &= \begin{bmatrix} 1 & 0 \\ 0 & 1 \end{bmatrix}, & X &= \begin{bmatrix} 0 & 1 \\ 1 & 0 \end{bmatrix}, \\
H &= \frac{\sqrt{2}}{2} \begin{bmatrix} 1 & 1 \\ 1 & -1 \end{bmatrix}, & R(\theta) &= \begin{bmatrix} \cos\theta & \sin\theta \\ \sin\theta & -\cos\theta \end{bmatrix}.
\end{aligned}
\tag{2}
$$

Controlled quantum gates are an important class of multiple quantum gates, Let U be a $2^m \times 2^m$ unitary matrix, the expression of $C_n^t(U)$ and $V_n^t(U)$ in Fig. 1 (c) and (d) are calculated by:

$$
\begin{cases}
C_n^t(U) = (|t\rangle\langle t|) \otimes U + \displaystyle\sum_{s=0,s\neq t}^{2^n-1} \left((|s\rangle\langle s|) \otimes I^{\otimes m} \right), \\
V_n^t(U) = U \otimes (|t\rangle\langle t|) + \displaystyle\sum_{s=0,s\neq t}^{2^n-1} \left(I^{\otimes m} \otimes (|s\rangle\langle s|) \right).
\end{cases}
\tag{3}
$$

(a)   (b)

(c)   (d)
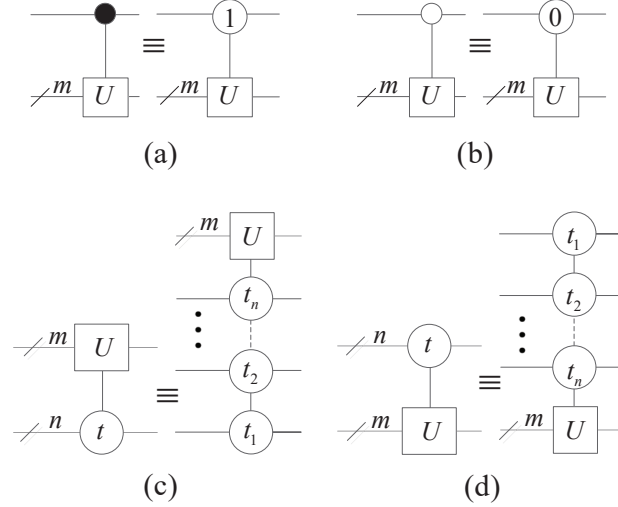
Fig. 1.   Graphical representation of quantum controlled circuits.   (a) $C_1^1(U)$.   (b)$C_1^0(U)$. (c)$C_n^t(U)$. (d)$V_n^t(U)$, the sequence $t = \sum_{i=1}^{n} t_i \times 2^{i-1}$ and $t_n, \cdots t_2, t_1 \in \{0,1\}$.

2.2   Log-polar coordinate sampling

Log-polar sampling is an important method [8] to convert rectangular coordinates (x, y) to log-polar coordinates (ρ, θ). The relationship between rectangular coordinates (x, y) and log-polar coordinates (ρ, θ) are depicted in Fig. 2 and expressed in Eq. (4).

$$\begin{cases} \rho = \log_{base}\sqrt{(x - x_c)^2 + (y - y_c)^2}, \\ \theta = \arctan\frac{y - y_c}{x - x_c}. \end{cases} \tag{4}$$

Where (x_c, y_c) represents the center pixel of log-polar sampling in rectangular coordinates. The symbol ρ denotes the log-radius and θ is the angle values after clockwise sampling. Where $base$ is the base of the logarithm. When $base = e$, the result of $\log_e =$ In. So Eq. (4) can be rewritten as:

$$\begin{cases} \rho^* = \text{In}\sqrt{(x - x_c)^2 + (y - y_c)^2}, \\ \theta = \arctan\frac{y - y_c}{x - x_c}. \end{cases} \tag{5}$$
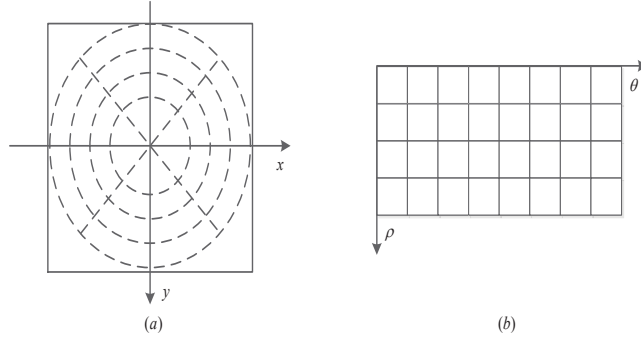

Fig. 2. The relationship between rectangular coordinates and log-polar coordinates. (a) An image on rectangular coordinate. (b) An image on log-polar coordinate.

2.3   Introduction of QUALPI

QUALPI [8] model is proposed for log-polar images, the log-radius ρ and angle values θ are assumed to be 2^m and 2^n respectively. $g(\rho, \theta)$ is the pixel value of the corresponding position (ρ, θ), which can be calculated by:

$$g(\rho, \theta) = C_0C_1\cdots C_{q-2}C_{q-1}, g(\rho, \theta) \in \left[0, 2^{q-1}\right]. \tag{6}$$

Where the sequence $C_0C_1\cdots C_{q-2}C_{q-1}$ is the binary expansion of grayscale $g(\rho, \theta)$, and $g(\rho, \theta) = \sum_{i=0}^{q-1} C_i \times 2^i, C_i \in \{0, 1\}$. The overall QUALPI is stored in a normalized state $|I\rangle$, which can be expressed as follows:

$$|I\rangle = \frac{1}{\sqrt{2^{m+n}}} \sum_{\rho=0}^{2^m-1} \sum_{\theta=0}^{2^n-1} (|g(\rho, \theta)\rangle \otimes |\rho\rangle \otimes |\theta\rangle). \tag{7}$$

Where $|\rho\rangle = |u_{m-1}u_{m-2}\cdots u_0\rangle$ and $|\theta\rangle = |v_{n-1}v_{n-2}\cdots v_0\rangle$ are the binary expansion of log-radius ρ and angle values θ, respectively. And $u_0, \cdots, u_{m-2}, u_{m-1}, v_0, \cdots, v_{n-2}, v_{n-1} \in \{0, 1\}$

For instance, the following state $|I_{\rho\theta}\rangle$ represents an image in Fig. 3 based on QUALPI.

$$
\begin{aligned}
|I_{\rho\theta}\rangle = \frac{1}{\sqrt{2^5}} \big[& |11111111\rangle \otimes (|00000\rangle + |00001\rangle + |00010\rangle + |00011\rangle \\
& + |00100\rangle + |00101\rangle + |00110\rangle + |00111\rangle) \\
+ & |00000000\rangle \otimes (|01000\rangle + |01001\rangle + |01010\rangle + |01011\rangle \\
& + |01100\rangle + |10101\rangle + |01110\rangle + |01111\rangle) \\
+ & |11111111\rangle \otimes (|10000\rangle + |10001\rangle + |10010\rangle + |10011\rangle \\
& + |10100\rangle + |10101\rangle + |10110\rangle + |10111\rangle) \\
+ & |00000000\rangle \otimes (|11000\rangle + |11001\rangle + |11010\rangle + |11011\rangle \\
& + |11100\rangle + |11101\rangle + |11110\rangle + |11111\rangle) \big].
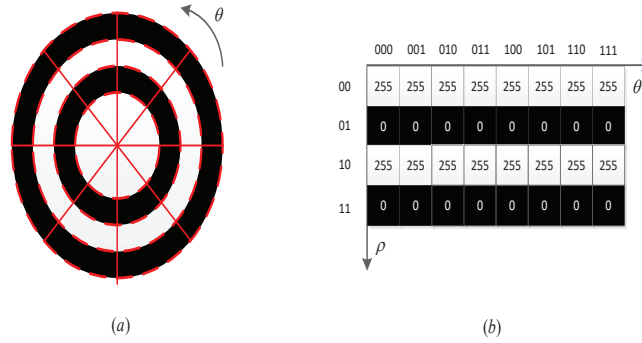\end{aligned}
\tag{8}
$$

Fig. 3. An example of QUALPI. (a) A 4×8 log-polar sampled image based on QUALPI. (b) The sampling distribution of (a) in θ and ρ directions.

3   A bit-plane representation for log-polar quantum images (BRLQI)

3.1   An improved log-polar coordinate sampling

In section 2.2, we briefly introduced log-polar coordinate sampling, It has two disadvantages to digital image processing [23]. (1) The image size changes after sampling. (2) The values of the logarithmic radius ρ and angle θ are no longer integers after sampling and differ from the pre-sampling values. In order to address this issue, We modify the Eq. (5) and give a new expression for the logarithmic polar coordinate sampling.

$$
\begin{cases}
\xi = floor(k_1 \rho^*) = floor(\frac{N}{\log(R_{\max})} \times \rho^*), \\
\varphi = floor(k_2 \theta) = floor(\frac{M}{2\pi} \times \theta).
\end{cases}
\tag{9}
$$

Where M and N denote the size of the original image in the rectangular coordinate system, respectively. The operation $floor()$ represents rounded down, such as $floor(1.5)=1$. The parameters ρ^* and θ are listed in Eq. (5), and $R_{\max}$ is the maximum value of the polar radius in logarithmic polar coordinates, which can be calculated by:

$$
R_{\max} = \sqrt{\left(\frac{M}{2}\right)^2 + \left(\frac{N}{2}\right)^2}.
\tag{10}
$$

Combining Eq. (9) and Eq. (10), it can be seen that the size of the image has not changed after the improved logarithmic polar coordinate sampling. During the sampling process, some pixels at the edge will be lost. and zero padding is used to deal with it. The purpose of applying the operation $floor()$ to the final result is to better encode digital images.

3.2   BRLQI for grayscale images

Each pixel in grayscale images can be illustrated by 8 bits binary sequence. Thus, a grayscale image can be decomposed into eight bit-planes, which can be shown in Fig. 4.

Fig. 4. Bit-planes decomposition of grayscale images.

Each bit plane of the grayscale image is represented as follows:

$$\left|\Psi^l\right\rangle = \frac{1}{\sqrt{2^h}} \sum_{\xi=0}^{2^{h-k}-1} \sum_{\phi=0}^{2^k-1} |f(\xi,\varphi,l)\rangle \, |\xi\rangle \, |\varphi\rangle. \tag{11}$$

Where l represents the $l-$th bit-plane, $l = 1, 2, \cdots, 8$, and $f(\xi,\varphi,l) \in \{0,1\}$. $|\xi\rangle = |\sigma_h \sigma_{h-1} \cdots \sigma_{k+1}\rangle$ and $|\varphi\rangle = |\sigma_k \sigma_{k-1} \cdots \sigma_1\rangle$ represent the improved logarithmic radius and rotation angle, respectively. $\sigma_1, \cdots, \sigma_{k-1}, \sigma_k, \sigma_{k+1}, \cdots, \sigma_{h-1}, \sigma_h \in \{0,1\}$,the sequences $\sigma_h \sigma_{h-1} \cdots \sigma_{k+1}$ and $\sigma_k \sigma_{k-1} \cdots \sigma_1$ are the binary expansion of φ and ξ in Eq. (9), respectively. For example, the least significant bit (LSB) of the image shown in subfigure (c) of Fig. 5, the state $\left|\Psi^1\right\rangle$ can be expressed as follows:

$$\begin{aligned}\left|\Psi^1\right\rangle = \tfrac{1}{4}(&|0\rangle\,|0\rangle\,|000\rangle + |0\rangle\,|0\rangle\,|001\rangle + |1\rangle\,|0\rangle\,|010\rangle + |1\rangle\,|0\rangle\,|011\rangle \\ &+ |0\rangle\,|0\rangle\,|100\rangle + |1\rangle\,|0\rangle\,|101\rangle + |1\rangle\,|0\rangle\,|110\rangle + |1\rangle\,|0\rangle\,|111\rangle \\ &+ |0\rangle\,|1\rangle\,|000\rangle + |0\rangle\,|1\rangle\,|001\rangle + |1\rangle\,|1\rangle\,|010\rangle + |1\rangle\,|1\rangle\,|011\rangle \\ &+ |0\rangle\,|1\rangle\,|100\rangle + |0\rangle\,|1\rangle\,|101\rangle + |0\rangle\,|1\rangle\,|110\rangle + |0\rangle\,|1\rangle\,|111\rangle).\end{aligned} \tag{12}$$

In order to combine the eight bit-planes of a grayscale image in one state, a BRLQI model is defined to represent a $2^{h-k} \times 2^k$ grayscale image as follows:

$$\begin{aligned}\left|\Psi_B^8\right\rangle &= \tfrac{1}{\sqrt{2^3}} \sum_{l=1}^{8} \left|\Psi^l\right\rangle |l\rangle \\ &= \frac{1}{\sqrt{2^{h+3}}} \sum_{l=1}^{8} \sum_{\xi=0}^{2^{h-k}-1} \sum_{\phi=0}^{2^k-1} |f(\xi,\varphi,l)\rangle \, |\xi\rangle \, |\varphi\rangle \, |l\rangle.\end{aligned} \tag{13}$$

Where $f(\xi,\varphi,l) \in \{0,1\}$, the variable l indicates the $l-$ th bit-plane. In particular, when $k = n$ and $h = m + k$, the Eq. (13) can be overwritten as below:

$$\begin{aligned}\left|\Psi_{BN}^8\right\rangle &= \tfrac{1}{\sqrt{2^3}} \sum_{l=1}^{8} \left|\Psi^l\right\rangle |l\rangle \\ &= \frac{1}{\sqrt{2^{m+n+3}}} \sum_{l=1}^{8} \sum_{\xi=0}^{2^m-1} \sum_{\phi=0}^{2^n-1} |f(\xi,\varphi,l)\rangle \, |\xi\rangle \, |\varphi\rangle \, |l\rangle.\end{aligned} \tag{14}$$

From Eq. (14), it is clear that BRLQI uses only $m+n+4$ qubits to depict a grayscale image. In contrast, the QUALPI model requires $m+n+8$ qubits to represent a grayscale image, so the storage capacity of BRLQI is 16 times greater than QUALPI. The implementation of the quantum circuit in Eq.(13) is shown in Fig. 6, and its equivalent simplified circuit is displayed in Fig. 7.
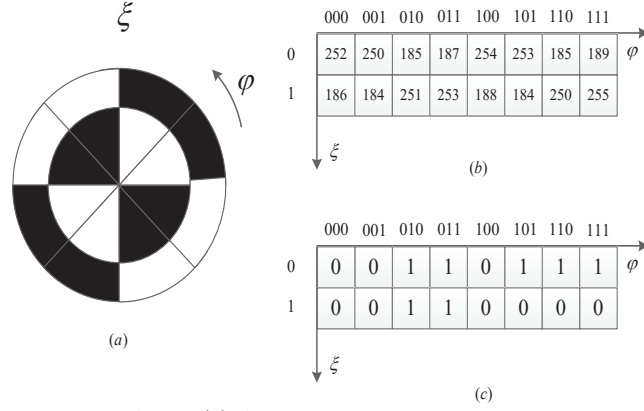
Fig. 5. An example of QUALPI. (a) A 2×8 log-polar sampled image based on QUALPI. (b) The sampling distribution of (a) in θ and ρ directions (i.e., h=4, k=3 and $f(\xi, \varphi) \in (0, 255)$). (c) The least significant bit (LSB) of the subfigure (a) based on BRLQI.(i.e., h=4, k=3 and $f(\xi, \varphi, l) \in \{0, 1\}$).

Fig. 6. The implementation circuit of BRLQI for grayscale images.

Fig. 7. The equivalent simplified circuit of BRLQI for grayscale images. The circuit in the red box is noted as U_G.

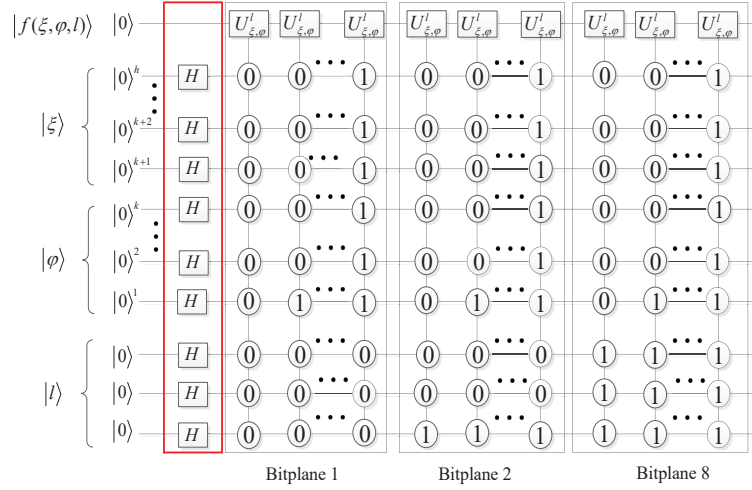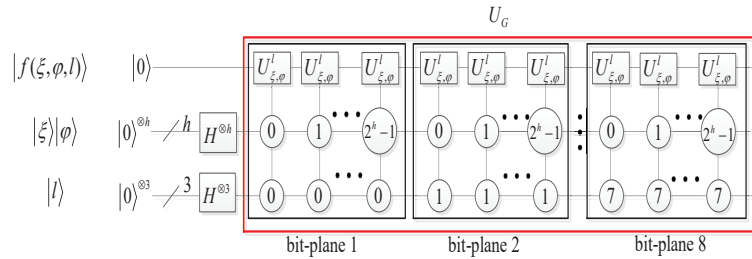### 3.3   Quantum state preparation for grayscale image of BRLQI

For the purpose of quantum image processing, we need to prepare an initial state for BRLQI. Applying Hadamard gates on the initial state $|0\rangle^{\otimes h+4}$, we obtain

$$
\begin{aligned}
|I_{initial}\rangle &= (I \otimes H^{\otimes h+3})|0\rangle^{\otimes h+4} \\
&= (I \otimes H^{\otimes h+3})(|0\rangle \otimes |0\rangle^{\otimes h+3}) \\
&= \frac{1}{\sqrt{2^{h+3}}} \sum_{l=1}^{8} \sum_{\xi=0}^{2^{h-k}-1} \sum_{\phi=0}^{2^{k}-1} |0\rangle |\xi\rangle |\varphi\rangle |l\rangle.
\end{aligned}
\tag{15}
$$

Where $|0\rangle^{\otimes h}$ is the h times tensor product of $|0\rangle$. Similarly, $H^{\otimes h+3}$ is the $h+3$ times tensor product of H. The quantum circuit implementation of this process is shown in the red boxed in Fig. 6. To set the value of the first quantum register, we define the operator $U_{\xi,\varphi}^{l}$, which can be expressed as follows:

$$
U_{\xi,\varphi}^{l} = (f(\xi,\varphi,l) \oplus 1)I + f(\xi,\varphi,l)X.
\tag{16}
$$

Where $\oplus$ is an exclusive-or operate. If $f(\xi,\varphi,l){=}0, U_{\xi,\varphi}^{l} = I$, otherwise, $U_{\xi,\varphi}^{l} = X$. The variable l represents the $l-$th bit-plane, $l = 1, 2, \cdots, 8$. According to Eq. (3), we define a unitary operator $V_{h+3}^{j}(U_{\xi,\varphi}^{l})$ for pixel assignment in the following equation:

$$
V_{h+3}^{j}(U_{\xi,\varphi}^{l}) = (U_{\xi,\varphi}^{l} \otimes |\xi\varphi l\rangle \langle \xi\varphi l|) + \sum_{j=0, j\neq\xi\varphi l}^{2^{h+3}-1} (I \otimes (|j\rangle \langle j|)).
\tag{17}
$$

Finally, by using the Eq. (17) with $j = 0, 1, \cdots, 2^{h+3} - 1$ successively on state $|I_{initial}\rangle$, we have

$$
\left[\prod_{j=0}^{2^{h+3}-1} V_{h+3}^{j}(U_{\xi,\varphi}^{l}) \right] |I_{initial}\rangle = \frac{1}{\sqrt{2^{h+3}}} \sum_{l=1}^{8} \sum_{\xi=0}^{2^{h-k}-1} \sum_{\phi=0}^{2^{k}-1} |f(\xi,\varphi,l)\rangle |\xi\rangle |\varphi\rangle |l\rangle = \left| \Psi_{B}^{8} \right\rangle.
\tag{18}
$$

Where the quantum state $|I_{initial}\rangle$ is listed in Eq. (15). Combining Eqs. (15), (17) and (18), a complete quantum grayscale image has been stored in the state $\left|\Psi_{B}^{8}\right\rangle$. The complete circuit of BRLQI for a $2^{h-k} \times 2^{k}$ grayscale image is shown in Fig. 7, and the red box in the circuit is noted as U_{G}. For instance, we show the grayscale image based on BRLQI in subfigure (b) of Fig. 5, and the corresponding quantum circuit implementation is displayed in Fig. 8.
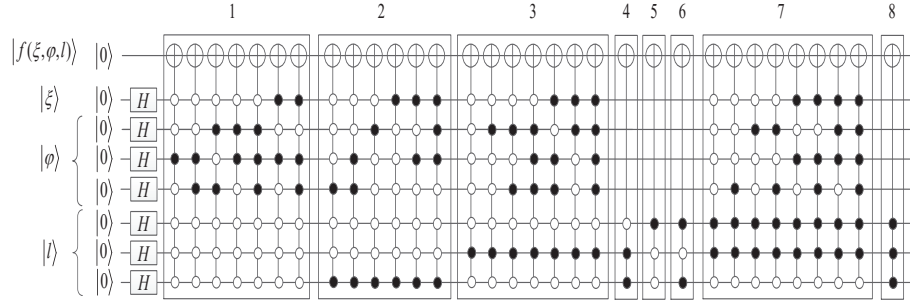
Fig. 8. The implementation circuit of BRLQI for grayscale images in subfigure (b) of Fig. 5. The circuit in the box represents the l − th bit-plane, where $l \in \{1, 2, 3, 4, 5, 6, 7, 8\}$.

The expression of $\left|\Psi^l\right\rangle$ for each bit-plane in Fig. 8 is expressed as below:

$$
\begin{cases}
\begin{aligned}
\left|\Psi^2\right\rangle =& \tfrac{1}{4}(|0\rangle\,|0\rangle\,|000\rangle + |1\rangle\,|0\rangle\,|001\rangle + |0\rangle\,|0\rangle\,|010\rangle + |1\rangle\,|0\rangle\,|011\rangle \\
& + |1\rangle\,|0\rangle\,|100\rangle + |0\rangle\,|0\rangle\,|101\rangle + |0\rangle\,|0\rangle\,|110\rangle + |0\rangle\,|0\rangle\,|111\rangle \\
& + |1\rangle\,|1\rangle\,|000\rangle + |0\rangle\,|1\rangle\,|001\rangle + |1\rangle\,|1\rangle\,|010\rangle + |0\rangle\,|1\rangle\,|011\rangle \\
& + |0\rangle\,|1\rangle\,|100\rangle + |0\rangle\,|1\rangle\,|101\rangle + |1\rangle\,|1\rangle\,|110\rangle + |0\rangle\,|1\rangle\,|111\rangle),
\end{aligned} \\[6pt]
\begin{aligned}
\left|\Psi^3\right\rangle =& \tfrac{1}{4}(|1\rangle\,|0\rangle\,|000\rangle + |0\rangle\,|0\rangle\,|001\rangle + |0\rangle\,|0\rangle\,|010\rangle + |0\rangle\,|0\rangle\,|011\rangle \\
& + |1\rangle\,|0\rangle\,|100\rangle + |1\rangle\,|0\rangle\,|101\rangle + |0\rangle\,|0\rangle\,|110\rangle + |1\rangle\,|0\rangle\,|111\rangle \\
& + |0\rangle\,|1\rangle\,|000\rangle + |0\rangle\,|1\rangle\,|001\rangle + |0\rangle\,|1\rangle\,|010\rangle + |1\rangle\,|1\rangle\,|011\rangle \\
& + |1\rangle\,|1\rangle\,|100\rangle + |0\rangle\,|1\rangle\,|101\rangle + |0\rangle\,|1\rangle\,|110\rangle + |1\rangle\,|1\rangle\,|111\rangle),
\end{aligned} \\[6pt]
\left|\Psi^4\right\rangle = \left|\Psi^5\right\rangle = \left|\Psi^6\right\rangle = \left|\Psi^8\right\rangle = \tfrac{1}{4}\sum_{\xi=0}^{1}\sum_{\varphi=0}^{3}|1\rangle\,|\xi\rangle\,|\varphi\rangle, \\[6pt]
\begin{aligned}
\left|\Psi^7\right\rangle =& \tfrac{1}{4}(|1\rangle\,|0\rangle\,|000\rangle + |1\rangle\,|0\rangle\,|001\rangle + |0\rangle\,|0\rangle\,|010\rangle + |0\rangle\,|0\rangle\,|011\rangle \\
& + |1\rangle\,|0\rangle\,|100\rangle + |1\rangle\,|0\rangle\,|101\rangle + |0\rangle\,|0\rangle\,|110\rangle + |0\rangle\,|0\rangle\,|111\rangle \\
& + |0\rangle\,|1\rangle\,|000\rangle + |0\rangle\,|1\rangle\,|001\rangle + |1\rangle\,|1\rangle\,|010\rangle + |1\rangle\,|1\rangle\,|011\rangle \\
& + |0\rangle\,|1\rangle\,|100\rangle + |0\rangle\,|1\rangle\,|101\rangle + |1\rangle\,|1\rangle\,|110\rangle + |1\rangle\,|1\rangle\,|111\rangle).
\end{aligned}
\end{cases}
\tag{19}
$$

Where the state $\left|\Psi^1\right\rangle$ is described in Eq.(12), since the pixel values in the 4th, 5th, 6th and 8th bit-planes are all one, their simplified quantum circuit is shown in Fig. 8.

3.4   BRLQI for color images

Since the RGB color image can be decomposed into three channels, it can be expressed as

$$
\begin{cases}
\left|\Psi_B^r\right\rangle = \frac{1}{\sqrt{2^{h+3}}} \sum_{l=1}^{8} \sum_{\xi=0}^{2^{h-k}-1} \sum_{\varphi=0}^{2^k-1} |f_r(\xi,\varphi,l)\rangle\,|\xi\rangle\,|\varphi\rangle\,|l\rangle, \\[6pt]
\left|\Psi_B^g\right\rangle = \frac{1}{\sqrt{2^{h+3}}} \sum_{l=1}^{8} \sum_{\xi=0}^{2^{h-k}-1} \sum_{\varphi=0}^{2^k-1} |f_g(\xi,\varphi,l)\rangle\,|\xi\rangle\,|\varphi\rangle\,|l\rangle, \\[6pt]
\left|\Psi_B^b\right\rangle = \frac{1}{\sqrt{2^{h+3}}} \sum_{l=1}^{8} \sum_{\xi=0}^{2^{h-k}-1} \sum_{\varphi=0}^{2^k-1} |f_b(\xi,\varphi,l)\rangle\,|\xi\rangle\,|\varphi\rangle\,|l\rangle.
\end{cases}
\tag{20}
$$

Where $f_r(\xi,\varphi,l), f_g(\xi,\varphi,l)$ and $f_b(\xi,\varphi,l) \in \{0, 1\}$. $\left|\Psi_B^r\right\rangle, \left|\Psi_B^g\right\rangle$ and $\left|\Psi_B^b\right\rangle$ are three channels of the color image respectively, each channel is regarded as a grayscale image and the corresponding quantum state $\left|\Psi_B^r\right\rangle, \left|\Psi_B^g\right\rangle, \left|\Psi_B^b\right\rangle$ can be prepared according to Eqs. (15)-(18).

The expression for the color image of the BRLQI model is defined as follows:

$$\left|\Psi_B^{24}\right\rangle = \frac{1}{\sqrt{3}}(\left|\Psi_B^r\right\rangle\left|01\right\rangle + \left|\Psi_B^g\right\rangle\left|10\right\rangle + \left|\Psi_B^b\right\rangle\left|11\right\rangle).\tag{21}$$

Where the quantum states $\left|01\right\rangle\left|10\right\rangle$ and $\left|11\right\rangle$ are used to encode the channel information of the color image, respectively. In order to realize the storage of the color image $\left|\Psi_B^{24}\right\rangle$, we design quantum circuits in Fig. 9.
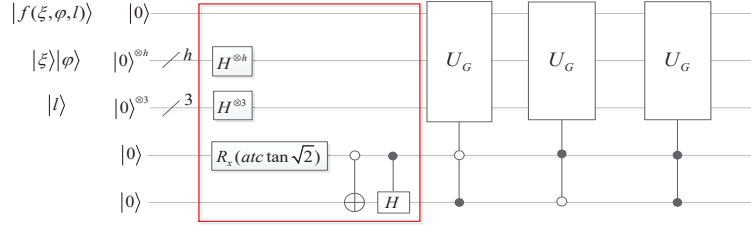

Fig. 9. The implementation circuit of BRLQI for color images.

The circuit in the red box in Fig. 9 implements the function

$$\begin{aligned}
\left|0\right\rangle\left|0\right\rangle^{\otimes h}\left|0\right\rangle^{\otimes 3}\left|0\right\rangle\left|0\right\rangle \rightarrow \frac{1}{\sqrt{3\times 2^{h+3}}}(\sum_{l=1}^{8}\sum_{\xi=0}^{2^{h-k}-1}\sum_{\varphi=0}^{2^k-1}\left|0\right\rangle\left|\xi\right\rangle\left|\varphi\right\rangle\left|l\right\rangle\left|01\right\rangle \\
+ \sum_{l=1}^{8}\sum_{\xi=0}^{2^{h-k}-1}\sum_{\varphi=0}^{2^k-1}\left|0\right\rangle\left|\xi\right\rangle\left|\varphi\right\rangle\left|l\right\rangle\left|10\right\rangle + \sum_{l=1}^{8}\sum_{\xi=0}^{2^{h-k}-1}\sum_{\varphi=0}^{2^k-1}\left|0\right\rangle\left|\xi\right\rangle\left|\varphi\right\rangle\left|l\right\rangle\left|11\right\rangle).
\end{aligned}\tag{22}$$

The controlled quantum gate circuit U_G stores the three-channel information of the color image and the specific circuit structure is shown in Fig. 7. Therefore, a color image is stored in a quantum state $\left|\Psi_B^{24}\right\rangle$ in Fig. 9 by using

$$\left|0\right\rangle\left|0\right\rangle^{\otimes h+3}\left|0\right\rangle^{\otimes 2} \rightarrow \left|\Psi_B^{24}\right\rangle.\tag{23}$$

From Eq.(21), we conclude that BRLQI uses $m+n+6$ qubits to depict a color image, which improves the deficiency that QUALPI can not be used for color images. For instance, we show the color image based on BRLQI in subfigure (b) of Fig. 10, the expressions for $\left|\Psi_B^r\right\rangle, \left|\Psi_B^g\right\rangle$ and $\left|\Psi_B^b\right\rangle$ in Fig. 10 are listed as below:

$$\begin{cases}
\left|\Psi_B^r\right\rangle = \frac{1}{\sqrt{2^3}}\sum_{l=1}^{8}\left|\Psi_r^l\right\rangle\left|l\right\rangle, \\
\left|\Psi_B^g\right\rangle = \frac{1}{\sqrt{2^3}}\sum_{l=1}^{8}\left|\Psi_g^l\right\rangle\left|l\right\rangle, \\
\left|\Psi_B^b\right\rangle = \frac{1}{\sqrt{2^3}}\sum_{l=1}^{8}\left|\Psi_b^l\right\rangle\left|l\right\rangle.
\end{cases}\tag{24}$$

Where $\left|\Psi_r^l\right\rangle, \left|\Psi_g^l\right\rangle$ and $\left|\Psi_b^l\right\rangle$ represent the bit-planes of the R, G, and B channels of the color image, respectively, where $l \in \{1,2,3,4,5,6,7,8\}$, and their expressions are defined in Eqs.

(25)-(27).

$$
\begin{aligned}
\left|\Psi_r^1\right\rangle &= \left|\Psi_r^2\right\rangle = \left|\Psi_r^3\right\rangle = \left|\Psi_r^4\right\rangle = \left|\Psi_r^5\right\rangle = \left|\Psi_r^6\right\rangle = \left|\Psi_r^7\right\rangle = \left|\Psi_r^8\right\rangle \\
&= \tfrac{1}{4}(|0\rangle\,|0\rangle\,|000\rangle + |1\rangle\,|0\rangle\,|001\rangle + |0\rangle\,|0\rangle\,|010\rangle + |1\rangle\,|0\rangle\,|011\rangle \\
&\quad + |0\rangle\,|0\rangle\,|100\rangle + |1\rangle\,|0\rangle\,|101\rangle + |0\rangle\,|0\rangle\,|110\rangle + |1\rangle\,|0\rangle\,|111\rangle \\
&\quad + |1\rangle\,|1\rangle\,|000\rangle + |0\rangle\,|1\rangle\,|001\rangle + |1\rangle\,|1\rangle\,|010\rangle + |0\rangle\,|1\rangle\,|011\rangle \\
&\quad + |1\rangle\,|1\rangle\,|100\rangle + |0\rangle\,|1\rangle\,|101\rangle + |1\rangle\,|1\rangle\,|110\rangle + |0\rangle\,|1\rangle\,|111\rangle).
\end{aligned} \tag{25}
$$

$$
\begin{aligned}
\left|\Psi_g^1\right\rangle &= \left|\Psi_g^2\right\rangle = \left|\Psi_g^3\right\rangle = \left|\Psi_g^4\right\rangle = \left|\Psi_g^5\right\rangle = \left|\Psi_g^6\right\rangle = \left|\Psi_g^7\right\rangle = \left|\Psi_g^8\right\rangle \\
&= \tfrac{1}{4} \sum_{\xi=0}^{1} \sum_{\varphi=0}^{3} |0\rangle\,|\xi\rangle\,|\varphi\rangle.
\end{aligned} \tag{26}
$$

$$
\begin{aligned}
\left|\Psi_b^1\right\rangle &= \left|\Psi_b^2\right\rangle = \left|\Psi_b^3\right\rangle = \left|\Psi_b^4\right\rangle = \left|\Psi_b^5\right\rangle = \left|\Psi_b^6\right\rangle = \left|\Psi_b^7\right\rangle = \left|\Psi_b^8\right\rangle \\
&= \tfrac{1}{4}(|1\rangle\,|0\rangle\,|000\rangle + |0\rangle\,|0\rangle\,|001\rangle + |1\rangle\,|0\rangle\,|010\rangle + |0\rangle\,|0\rangle\,|011\rangle \\
&\quad + |1\rangle\,|0\rangle\,|100\rangle + |0\rangle\,|0\rangle\,|101\rangle + |1\rangle\,|0\rangle\,|110\rangle + |0\rangle\,|0\rangle\,|111\rangle \\
&\quad + |0\rangle\,|1\rangle\,|000\rangle + |1\rangle\,|1\rangle\,|001\rangle + |0\rangle\,|1\rangle\,|010\rangle + |1\rangle\,|1\rangle\,|011\rangle \\
&\quad + |0\rangle\,|1\rangle\,|100\rangle + |1\rangle\,|1\rangle\,|101\rangle + |0\rangle\,|1\rangle\,|110\rangle + |1\rangle\,|1\rangle\,|111\rangle).
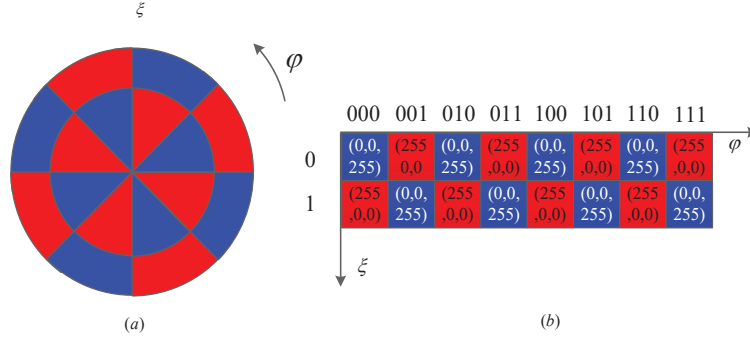\end{aligned} \tag{27}
$$

Fig. 10. An example of BRLQI for color image. (a) A 2×8 log-polar sampled image based on BRLQI. (b) The sampling distribution of (a) in φ and ξ directions.(i.e., h=4, k=3 and $f_r(\xi,\varphi), f_g(\xi,\varphi), f_b(\xi,\varphi) \in (0,255)$, Where $f_r(\xi,\varphi), f_g(\xi,\varphi)$, and $f_b(\xi,\varphi)$ represent the colour components of the three channels R, G and B of the image respectively). The correspondence between $f_r(\xi,\varphi)$ and $f_r(\xi,\varphi,l)$, $f_g(\xi,\varphi)$ and $f_g(\xi,\varphi,l)$, $f_b(\xi,\varphi)$ and $f_b(\xi,\varphi,l)$ is satisfied $f_r(\xi,\varphi) = \sum_{l=1}^{8} f_r(\xi,\varphi,l) \times 2^{l-1}, f_g(\xi,\varphi) = \sum_{l=1}^{8} f_g(\xi,\varphi,l) \times 2^{l-1}, f_b(\xi,\varphi) = \sum_{l=1}^{8} f_b(\xi,\varphi,l) \times 2^{l-1}$. Where $f_r(\xi,\varphi,l), f_g(\xi,\varphi,l), f_b(\xi,\varphi,l) \in \{0,1\}$

3.5 Image retrieval based on BRLQI

Quantum measurement is an effective way to obtain classical information from a quantum state, and the superposition state collapses to the basic state with some probability after the measurement operation [24]. Therefore many identical quantum states need to be prepared simultaneously for quantum measurements, the complexity of preparing quantum states is polynomial [8]. We define measurement operators M_g and M_c to implement image retrieval from quantum states. The expression of M_g is defined as below

$$
\begin{cases}
M_g = \sum_{i=0}^{2^{h+3}-1} \lambda_i P_i, \\
P_i = |i\rangle\,\langle i|.
\end{cases} \tag{28}
$$

Where P_i is the projection on the feature space M_g, and the corresponding eigenvalue is denoted as λ_i . The state $|i\rangle$ and its dual state $\langle i|$ are $|i\rangle = |\xi\rangle |\varphi\rangle |l\rangle$ and $\langle i| = \langle\xi| \langle\varphi| \langle l|$, respectively. Where $\xi \in \left\{0, 1, 2, \cdots, 2^{h-k} - 1\right\}, \varphi \in \left\{0, 1, 2, \cdots, 2^k - 1\right\}$, and $l \in \{1, 2, \cdots, 8\}$.

Applying the operator M_g to the quantum state $\left|\Psi_B^8\right\rangle$ in Eq. (13), the coordinate state $|\xi\rangle |\varphi\rangle$ in the $l - $th bit-plane can be obtained with the following probability

$$p(\lambda_i) = \left\langle\Psi_B^8\right| P_i \left|\Psi_B^8\right\rangle = \frac{1}{2^{h+3}}. \tag{29}$$

After the quantum state $\left|\Psi_B^8\right\rangle$ is measured, it will evolve into

$$\frac{P_i \left|\Psi_B^8\right\rangle}{\sqrt{p(i)}} = |\lambda_i\rangle |\xi\rangle |\theta\rangle |l\rangle . \tag{30}$$

Therefore, a grayscale image with size $2^{h-k} \times 2^k$ based on BRLQI is retrieved after $O(2^{h+3})$ measurements. Similar to Eq. (28), we define the observable operator M_c as follows:

$$\begin{cases} M_c = \sum\limits_{j=0}^{2} \lambda_j P_j, \\ P_j = I^{\otimes h+4} \otimes |j\rangle \langle j| . \end{cases} \tag{31}$$

After performing the observation operator M_c, the quantum state $\left|\Psi_B^{24}\right\rangle$ collapses to one of the three states $\left\{ \left|\Psi_b^r\right\rangle, \left|\Psi_b^g\right\rangle, \left|\Psi_b^b\right\rangle \right\}$ with probability 1/3. Then, we use the measurement operator M_g in Eq. (28) to retrieve three grayscale images from $\left|\Psi_b^r\right\rangle, \left|\Psi_b^g\right\rangle$, and $\left|\Psi_b^b\right\rangle$. Therefore, a color image with size $2^{h-k} \times 2^k$ based on BRLQI is retrieved after $O(2^{h+3})$ measurements.

4   Quantum image processing based on BRLQI

In this section, we propose some circuit operations based on BRLQI for image processing. A grayscale image is used as an example to verify the feasibility of these operations. The simulation experiments are carried out on Matlab R2017a with a windows 7 environment and 128G of RAM.

4.1   *color information complement operation*

From Eq. (13), the BRLQI model uses one qubit to represent the color information, so a NOT gate can be used to implement the complementary operation of an image with size $2^{h-k} \times 2^k$, i.e., the complement operation U_C is defined as follows:

$$U_C = X \otimes I^{\otimes h+3}. \tag{32}$$

Where X and I denote NOT gate and identity gate, respectively. Their expressions are given in Eq. (2). By using the operation U_C on the state $\left|\Psi_B^8\right\rangle$ in Eq. (13), we get the following result:

$$\begin{aligned} U_C \left|\Psi_B^8\right\rangle &= (X \otimes I^{\otimes h+3}) \frac{1}{\sqrt{2^3}} \sum_{l=1}^{8} \left|\Psi^l\right\rangle |l\rangle , \\ &= \frac{1}{\sqrt{2^{h+3}}} \sum_{l=1}^{8} \sum_{\xi=0}^{2^{h-k}-1} \sum_{\varphi=0}^{2^k-1} |1 - f(\xi, \varphi, l)\rangle |\xi\rangle |\varphi\rangle |l\rangle . \end{aligned} \tag{33}$$

The complete quantum circuit implementation is shown in Fig. 11.

(a)   (b)   (c)

Fig. 11. The operation U_C based on BRLQI. (a) The implementation circuit of U_C. (b) A 64×64 grayscale image. (c) The result of the complement operation U_C.

4.2 Reverse operation of bit-planes

The BRLQI model encodes eight bit-planes with three qubits, so the reverse operation of bit-planes can be implemented with three NOT gates. We define the bit-planes reversing operation U_R as follows:

$$U_R = I^{\otimes h+1} \otimes X^{\otimes 3}. \tag{34}$$

Similarly with Eq.(33), applying U_R to the state $\left|\Psi_B^8\right\rangle$, the following output can be obtained:

$$
\begin{aligned}
U_R \left|\Psi_B^8\right\rangle &= (I^{\otimes h+1} \otimes X^{\otimes 3}) \tfrac{1}{\sqrt{2^3}} \sum_{l=1}^{8} \left|\Psi^l\right\rangle \left|l\right\rangle, \\
&= \tfrac{1}{\sqrt{2^3}} \sum_{l=1}^{8} \left|\Psi^l\right\rangle \left|8-l\right\rangle, \\
&= \tfrac{1}{\sqrt{2^{h+3}}} \sum_{l=1}^{8} \sum_{\xi=0}^{2^{h-k}-1} \sum_{\varphi=0}^{2^k-1} \left|f(\xi,\varphi,l)\right\rangle \left|\xi\right\rangle \left|\varphi\right\rangle \left|8-l\right\rangle.
\end{aligned}
\tag{35}
$$

The specific quantum circuit is depicted in Fig. 12, which implements reverse order of bit-planes of a grayscale image of size $2^{h-k} \times 2^k$. Meanwhile, the results for each bit plane are shown in Fig. 13.
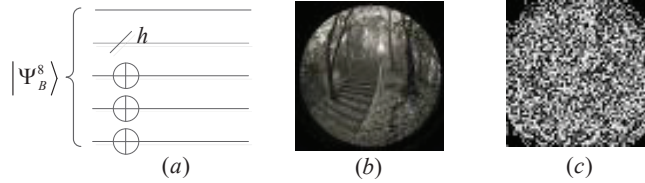

(a)   (b)   (c)

Fig. 12. The operation U_R based on BRLQI. (a) The implementation circuit of U_R. (b) A 64×64 grayscale image. (c) The result of the complement operation U_R.

4.3 Conditional exchange operations between bit-planes

Since the BRLQI model requires only one qubit to store the color information and its only possible values are 0 or 1. Therefore, we use the swap gates in Fig. 14 and the controlled quantum gates in Fig. 1 (a) and (b) to define the following controlled exchange gate operation U_T.

$$
\begin{cases}
U_T = C_1^1(U_1)C_1^0(U_0) = \left|0\right\rangle\left\langle 0\right| \otimes U_0 + \left|1\right\rangle\left\langle 1\right| \otimes U_1, \\
U_0 = I^{\otimes h} \otimes Swap(3), \\
U_1 = I^{\otimes h+1} \otimes Swap.
\end{cases}
\tag{36}
$$

| The 1-th bit-plane | The 1-th bit-plane | The 2-th bit-plane | The 3-th bit-plane |

| The 5-th bit-plane | The 6-th bit-plane | The 7-th bit-plane | The 8-th bit-plane |

Fig. 13. The result of the operation U_R for each bit-planes in Figure 12.

Fig. 14. Quantum swap gate circuits. (a) The gate. (b) The gate.

The circuit of U_T is designed in Fig. 15 (a) to realize the following functions:

$$\begin{cases} |l_2l_1l_0\rangle \leftrightarrow |l_2l_0l_1\rangle \,, & \text{when} \quad f(\xi,\varphi,l)=1, \\ |l_2l_1l_0\rangle \leftrightarrow |l_0l_1l_2\rangle \,, & \text{when} \quad f(\xi,\varphi,l)=0. \end{cases} \tag{37}$$

Where $|l_2l_1l_0\rangle$ denotes the bit-plane encoding of the original image and the subscript of the number l decreases gradually from top to bottom. By performing the operation U_T on the state $\left|\Psi_B^8\right\rangle$, the simulation result are shown in Fig. 15 (c) and Fig. 16, respectively.

Fig. 15. The operation U_T based on BRLQI. (a) The implementation circuit of U_T. (b) A 64×64 grayscale image. (c) The result of the complement operation U_T.

4.4   *Translation operation of bit-planes*

The bit-plane translation can be divided into left translation and right translation according to the translation order, and since the effects of both are equivalent, here we give the operation U_{RS} for right translation of bit-planes.

$$U_{RS} = (I^{\otimes h+3} \otimes X)(I^{\otimes h+2} \otimes V_1^1(X))(I^{\otimes h+1} \otimes V_2^3(X)). \tag{38}$$

The 1-th bit-plane   The 2-th bit-plane   The 3-th bit-plane   The 4-th bit-plane

The 5-th bit-plane   The 6-th bit-plane   The 7-th bit-plane   The 8-th bit-plane
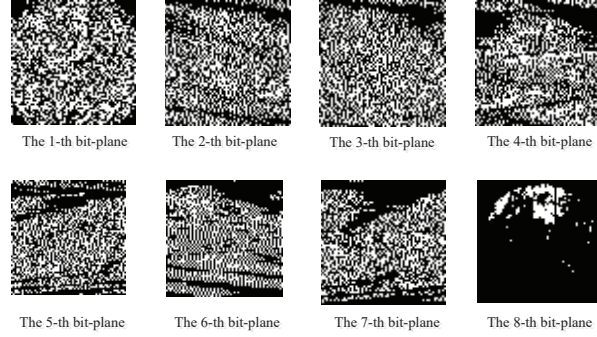
Fig. 16. The result of the operation U_T for each bit-planes in Figure 14.

Where $V_2^3(X)$ and $V_1^1(X)$ are displayed in Fig . 17, and their matrices are represented as follows:

$$V_2^3(X) = \begin{bmatrix} 1 & 0 & 0 & 0 & 0 & 0 & 0 & 0 \\ 0 & 1 & 0 & 0 & 0 & 0 & 0 & 0 \\ 0 & 0 & 1 & 0 & 0 & 0 & 0 & 0 \\ 0 & 0 & 0 & 0 & 0 & 0 & 0 & 0 \\ 0 & 0 & 0 & 0 & 1 & 0 & 0 & 0 \\ 0 & 0 & 0 & 0 & 0 & 1 & 0 & 0 \\ 0 & 0 & 0 & 0 & 0 & 0 & 1 & 0 \\ 0 & 0 & 0 & 1 & 0 & 0 & 0 & 0 \end{bmatrix}, V_1^1(X) = \begin{bmatrix} 1 & 0 & 0 & 0 \\ 0 & 0 & 0 & 1 \\ 0 & 0 & 1 & 0 \\ 0 & 1 & 0 & 0 \end{bmatrix}. \tag{39}$$

Applying the operation U_{RS} to the state $\left|\Psi_B^8\right\rangle$ in Eq.(13), we have

$$U_{RS}\left|\Psi_B^8\right\rangle = \frac{1}{\sqrt{2^3}} \sum_{l=1}^{8} \left|\Psi^l\right\rangle \left|l \bmod 8\right\rangle. \tag{40}$$

Where the mod is a modulo operation, the corresponding quantum circuit and simulation results are shown in Fig. 17 (a) and Fig. 18 respectively.

(a)   (b)   (c)
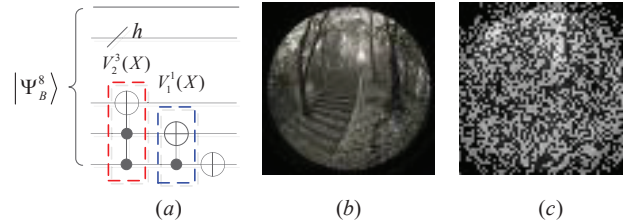
Fig. 17. The operation U_{RS} based on BRLQI. (a) The implementation circuit of U_{RS}. (b) A 64×64 grayscale image. (c) The result of the complement operation U_{RS}.

4.5   Grayscale image scrambling circuit based on BRLQI.

Combining the above operations, we define the overall circuit for grayscale image scrambling as follows:

$$U_{GA} = U_R U_C U_T U_{RS}. \tag{41}$$

The 1-th bit-plane   The 2-th bit-plane   The 3-th bit-plane   The 4-th bit-plane

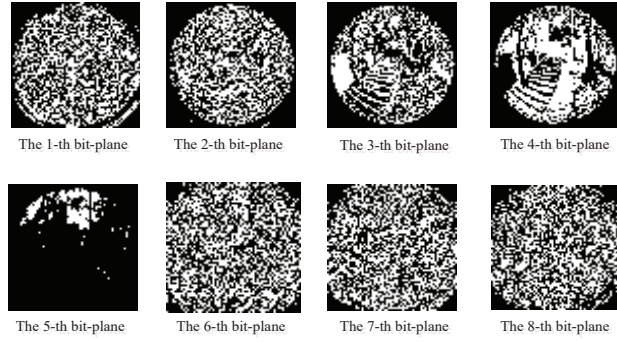The 5-th bit-plane   The 6-th bit-plane   The 7-th bit-plane   The 8-th bit-plane

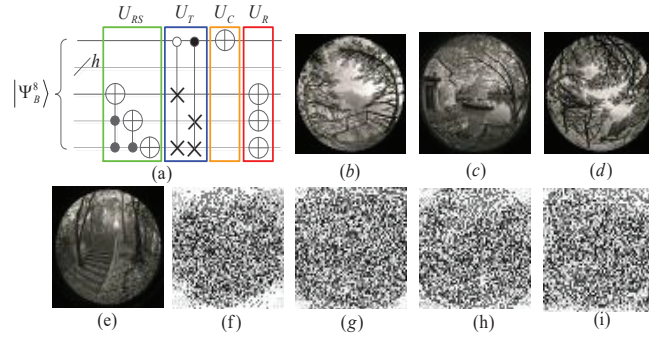Fig. 18. The result of the operation U_{RS} for each bit-planes in Figure 17.

Fig. 19. Scrambling results for grayscale images based on BRLQI. (a) The complete structure of the scrambling circuit U_{GA}. Where subplots (b)-(e) are the original grayscale images and (f)-(j) are the corresponding transformed images.
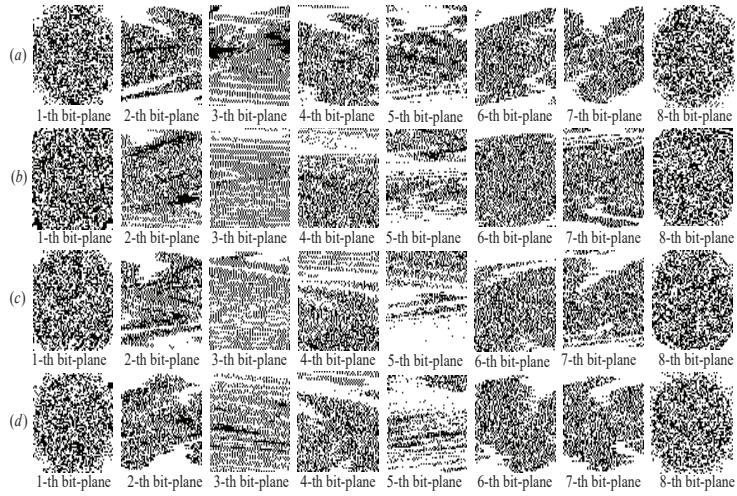

Fig. 20. The result of the operation U_{GA} for each bit-planes in Figure 19.

Which is realized by the quantum circuit in Fig. 19 (a).

The simulation results of Fig. 19 and Fig. 20 show that the image scrambling algorithm is effective, and the information of each bit-plane is hidden.

4.6 Color image scrambling circuit based on BRLQI

To modify the operation U_{GA}, we define the scrambling operation U_{GA} suitable for color images.

$$U_{CA} = U_{GA} \otimes I^{\otimes 2}. \tag{42}$$

Similarly, we define four operations $U_R^C, U_C^C, U_T^C, U_{RS}^C$ for color images

$$\begin{cases} U_R^C = U_R \otimes I^{\otimes 2}, \\ U_C^C = U_C \otimes I^{\otimes 2}, \\ U_T^C = U_T \otimes I^{\otimes 2}, \\ U_{RS}^C = U_{RS} \otimes I^{\otimes 2}. \end{cases} \tag{43}$$

From Eqs. (41) and (43), the Eq. (42) can be rewritten as
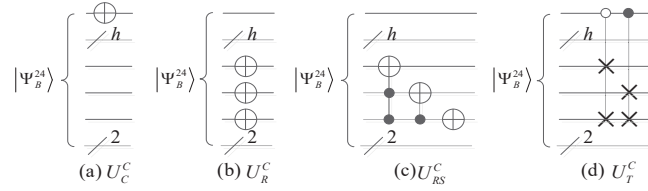
$$U_{CA} = U_R^C U_C^C U_T^C U_{RS}^C \tag{44}$$

Fig. 21. Four operational quantum circuits for color images. (a) The operation of U_C^C. (b) The operation of U_R^C. (c) The operation of U_{RS}^C. (d) The operation of U_T^C.

Applying four operations in Eqs. (43) to the state $\left| \Psi_B^{24} \right\rangle$ in Eq. (21), we obtain

$$\begin{cases} U_R^C \left| \Psi_B^{24} \right\rangle = \frac{1}{\sqrt{3}} (U_R \left| \Psi_B^r \right\rangle |01\rangle + U_R \left| \Psi_B^g \right\rangle |10\rangle + U_R \left| \Psi_B^b \right\rangle |11\rangle), \\ U_C^C \left| \Psi_B^{24} \right\rangle = \frac{1}{\sqrt{3}} (U_C \left| \Psi_B^r \right\rangle |01\rangle + U_C \left| \Psi_B^g \right\rangle |10\rangle + U_C \left| \Psi_B^b \right\rangle |11\rangle), \\ U_T^C \left| \Psi_B^{24} \right\rangle = \frac{1}{\sqrt{3}} (U_T \left| \Psi_B^r \right\rangle |01\rangle + U_T \left| \Psi_B^g \right\rangle |10\rangle + U_T \left| \Psi_B^b \right\rangle |11\rangle), \\ U_{RS}^C \left| \Psi_B^{24} \right\rangle = \frac{1}{\sqrt{3}} (U_{RS} \left| \Psi_B^r \right\rangle |01\rangle + U_{RS} \left| \Psi_B^g \right\rangle |10\rangle + U_{RS} \left| \Psi_B^b \right\rangle |11\rangle). \end{cases} \tag{45}$$

Where $U_R^C, U_C^C, U_T^C, U_{RS}^C$ are the complement, reverse, conditional exchange, translation, operations for RGB color images, respectively. And their circuits are designed in Fig. 21. The quantum state $\left| \Psi_B^{24} \right\rangle$ represents a color image in Eq. (21).

From Eq. (44), we can conclude that the operation U_{CA} is obtained by arranging the above four operations in a certain order. We use the operation U_{CA} to a 64×64 color image, the quantum circuit implementation and the simulation results are displayed in Figs. 22. For each of bit-planes, the results are depicted in Fig. 23.
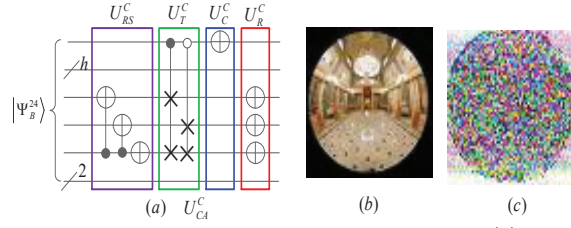
Fig. 22. Scrambling results for grayscale images based on BRLQI. (a) The complete structure of the scrambling circuit U_{CA}. Where subplots (a)-(d) are the original grayscale images and (f)-(j) are the corresponding transformed images.
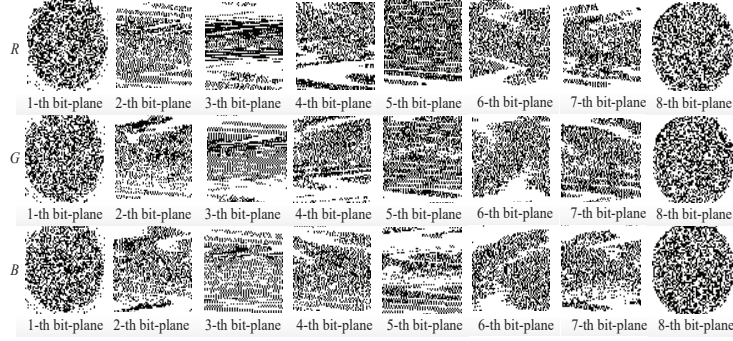

Fig. 23. The result of the operation U_{CA} for each bit-planes in Figure 22.

4.7   Comparative analysis of quantum operations between BRLQI and QUALPI

For different quantum operations, quantum cost (i.e., time complexity) is considered to be a key performance indicator. Some related research work[25][26] has shown that the quantum cost of the CNOT gate is 1, and its cost is much higher than that of the NOT gate. For instance, Assume that the cost of NOT gate is δ, and it satisfies $\delta \leq 1$.We list the cost of basic gates that used in this paper in Table. 1.

Table 1. The costs of some basic gates

Gate	Cost
CNOT gate	1
Fredkin gate[27]	5
Toffoli gate[1]	5
Swap gate	3
NOT gate	$\delta \ll 1$

Next, we present the quantum operations proposed in this paper and analyze the quantum cost of performing the same operations for both the BRLQI model and the QUALPI model.

For QUALPI, the circuits for the operation of color information complement, bit-planes reversing and bit-planes translation are shown in subfigures (a), (b), and (c) of Fig. 24, respectively. However, the quantum operation defined in Section 4.3 is difficult to effectively implement for other quantum image representation models.
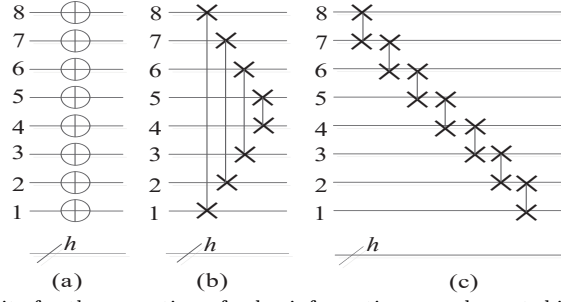
Fig. 24. The circuits for the operation of color information complement, bit-planes reversing and bit-planes translation for QUALPI.

Table 2. The costs of some image processing operations for QUALPI and BRLQI

Operation	QUALPI [8]	BRLQI
Color information complement operation U_C	8 δ	δ
Bit-planes reversing operation U_R	12	3 δ
Bit-planes translation operation U_{RS}	21	$6 + \delta \approx 6$
Color information complement operation U_C^C	$-$	δ
Bit-planes reversing operation U_R^C	$-$	3 δ
Bit-planes translation operation U_{RS}^C	$-$	$6 + \delta \approx 6$
U_T and U_T^C	$-$	10
U_{GA} and U_{CA}	$-$	$16 + 5\delta \approx 16$

From Table 2 and Fig. 24, we have collated the quantum costs of these operations in Table 3. Where the symbol "-" denotes the absence of data.

It is clearly that the quantum image representation of BRLQI has lower quantum cost than QUALPI, the main reason for this is that this paper uses a joint bit-plane and pixel encoding method, which makes the encoding of images more efficient. At the same time, the circuit designed in this paper can realize the scrambling of color and grayscale images, and can be used for image information encryption, video information encryption and other fields.

4.8   Comparison between QUALPI and BRLQI

We compare two image representation models QUALPI and BRLQI in polar coordinates, for grayscale images (GI), The storage capacity of BRLQI is 16 times higher than that of QUALPI. Furthermore, BRLQI is also used to represent color images (CI).

Table 3. The costs of some image processing operations for QUALPI and BRLQI

QIR	Qubits (GI)	Qubits (CI)	Image size	Pixel encoding
QUALPI[8]	$2n+8$	$-$	$2^{2n-k} \times 2^k$	Basis states
BRLQI	$2n+4$	$2n+6$	$2^{2n-k} \times 2^k$	Basis states

5   Conclusion

In this paper, we proposed a method BRLQI for quantum image representation based on bit-planes, which is applicable to log-polar coordinate systems. BRLQI uses $(n + 4)$ and $(n + 6)$ qubits to represent grayscale and color images with a size of $2^k \times 2^{n-k}$, respectively.

Compared with the model of QUALPI, the storage capacity of BRLQI enhances 16 times for grayscale images. Meanwhile, the model of QUALPI can also be used for color images, which is a significant advantage. Furthermore, we designed a sort of quantum circuits of BRLQI to verify our method by using Matlab, and the final result indicted that the original image information was successfully stored in a quantum state as a column vector. Through specific measurement operators, grayscale or color images can be retrieved from the quantum state.

In order to realize information hiding, we have designed the following types of operations, including color information complement operation, bit-planes reversing operation, bit-planes translation operation and conditional exchange operations between bit-planes. Combining the above operations, we designed quantum image scrambling circuits for grayscale and color images, respectively, and the simulation results show that the scrambling results are effective. At the same time, we present a quantum cost analysis of the above operations, which shows that the BRLQI algorithm has a lower algorithmic complexity compared with similar algorithms. In general, the quantum image representation method of logarithmic polar coordinates has many problems that need to be further studied. For example, how to implement adaptive sampling to resolve sampling non-uniformity is crucial for quantum image coding [28]. In addition, the rotation and scale transformation operations in log-polar coordinates are particularly important for the realization of complex image operations.

Acknowledgements

References

1. M. A. Nielsen, I. L. Chuang, *Quantum Computation and Quantum Information*. Cambridge: Cambridge University Press, 2000.
2. S. E. Venegas-Andraca, S. Bose, *Storing, processing, and retrieving an image using quantum mechanics*. Proceedings of the SPIE Conference on Quantum Information and Computation. pp. 137-14, 2003.
3. Feynman, R. P. *Simulating physics with computers*. Int. J. Theor. Phys., vol. 21, no. 6, pp. 467-488, 1982.
4. S. E. Venegas-Andraca, J. L. Ball, *Processing images in entangled quantum systems*. Quantum Inf. Process. vol. 9, no. 1, pp. 1-11, 2010.
5. P. Q. Le, F. Dong, and K.Hirota, *A flexible representation of quantum images for polynomial preparation, image compression, and processing operations*. Quantum Inf. Process. vol. 10, no. 1, pp. 63-84, 2011.
6. B. Sun, A. M. Iliyasu, F. Yan, F. Dong, and K. Hirota, *An RGB multi-channel representation for images on quantum computers*. Adv. Comput. Intell. inform. vol. 17, no.3, pp. 404-417, 2013.
7. H. S. Li, Q. Zhu, R. G. Zhou, *et.al.*, *Multi-dimensional color image storage and retrieval for a normal arbitrary quantum superposition state*. Quantum inf. Process. vol. 13, no. 4, pp. 991-1011, 2014.

8. Y. Zhang, K. Lu, Y. Gao, K. Xu. *A novel quantum representation for log-polar images.* Quantum Inf. Process, vol.12, no.5, pp. 3103-3126, 2013.

9. N. Jiang, L. Wang, *Quantum image scaling using nearest neighbor interpolation.* Quantum Inf. Process. vol. 14, no.5, pp. 1559-1571, 2015.

10. H. S. Li, P. Fan, H. Y. Xia, *et.al.*, *A Quantum Image Representation Based on Bit-planes.* IEEE Trans Circuits Syst I: Reg Papers, vol. 99, pp. 1-14, 2018.

11. H. S. Li, X. Chen, H. Y. Xia, *et.al.*, *Strongly trapped two-dimensional quantum walks.* IEEE Access, vol. 6, pp.62396-62404, 2018.

12. Wang L, Ran Q, Ma J, *et.al.*, *QRCI: A new quantum representation model of color digital images.* Optics Communications, vol. 438, pp.147-158, 2019.

13. Y. Zhang, K. Lu, Y. Gao, and M. Wang, *NEQR: a novel enhanced quantum representation of digital images.* Quantum Inf. Process., vol. 12, no. 8, pp. 2833-2860, 2013.

14. A. Grigoryan, S. Agaian, *New look on quantum representation of images: Fourier transform representation.* Int. Soc. Opt. Photonics, vol.19, no.5, pp. 126, 2020.

15. Yan F, Li N, Hirota K. *QHSL: A Quantum Hue, Saturation, and Lightness Color Model.* Information Sciences, vol.577, no.4, pp. 196-213, 2021.

16. S. Falkner, S. Y. *et.al.*, *Design of Threshold Segmentation Method for Quantum Image.* Int. J. Theor. Phys., vol.19, pp. 514538, 2020, doi: https://doi.org/10.1007/s10773-019-04346-7.

17. Jiang, N., Dang, Y. & Wang, J. *Quantum image matching.* . Quantum Inf. Process, vol.15, no.9, pp.35433572, 2016. doi: https://doi.org/10.1007/s11128-016-1364-2.

18. W. Hu, R. Zhou, A. El-Rafei and S. Jiang, *Quantum Image Watermarking Algorithm Based on Haar Wavelet Transform.* IEEE Access, vol. 7, pp. 121303-121320, 2019, doi: 10.1109/ACCESS.2019.2937390.

19. Zhou, R. G., *et.al.*, *Quantum color image watermarking based on Arnold transformation and LSB steganography.* International Journal of Quantum Information, vol.16, no.3, pp. 1850021, 2018, doi: 10.1142/S0219749918500211.

20. Z. Qu, Z. Li, G. Xu, S. Wu and X. Wang, *Quantum Image Steganography Protocol Based on Quantum Image Expansion and Grover Search Algorithm.* IEEE Access, vol. 7, pp. 50849-50857, 2019, doi: 10.1109/ACCESS.2019.2909906.

21. Lei, *et.al.*, *Novel quantum image encryption using one-dimensional quantum cellular automata.* Information Sciences: An International Journal, vol. 345, pp. 257-270, 2016.

22. Jiang, N., Dong, X., Hu, H. *et.al.*, *Quantum Image Encryption Based on Henon Mapping.* Int. J. Theor. Phys., vol.58, no.3, pp.979991, 2019, doi: https://doi.org/10.1007/s10773-018-3989-7.

23. Guo Y C, He W H, Gao C. *A frequency-domain image registration algorithm using the improved polar transform.* Journal of Chongqing University, vol.35, no.2, pp. 98-104, 2012.

24. Le P Q, Dong F, Hirota K. *A flexible representation of quantum images for polynomial preparation, image compression, and processing operations.* Quantum Inf. Process, vol.10, no.1, pp.63-84, 2011.

25. J. A. Smolin, D. P. DiVincenzo, *Five two-bit quantum gates are sufficient to implement the quantum Fredkin gate.* Phys. Rev. A ., vol. 53, no. 4, pp. 2855, 1996.

26. W. N. Hung, X. Song, G. Yang, *et.al.*, *Optimal synthesis of multiple output Boolean functions using a set of quantum gates by symbolic reachability analysis.* IEEE Trans Comput -Aided Des Integr Circuits Syst, vol. 25, pp.1652-1663, 2006.

27. N. Jiang, L. Wang, and W. Y. Wu, *Quantum Hilbert image scrambling.* Int. J. Theor. Phys., vol. 53, no. 7, pp. 2463-2484, 2014.

28. Vatsavayi V K, Kondaveeti H K. *Efficient ISAR Image Classification Using MECSM Representation.* Journal of King Saud University - Computer and Information Sciences, vol. 30, no. 3, pp. 356-372, 2018.